JACS
JOURNAL OF THE AMERICAN CHEMICAL SOCIETY

Article

pubs.acs.org/JACS

Thermally Robust $Au_{99}(SPh)_{42}$ Nanoclusters for Chemoselective Hydrogenation of Nitrobenzaldehyde Derivatives in Water

Gao Li, Chenjie Zeng, and Rongchao Jin*

Department of Chemistry, Carnegie Mellon University, Pittsburgh, Pennsylvania 15213, United States

Supporting Information

ABSTRACT: We report the synthesis and catalytic application of thermally robust gold nanoclusters formulated as $Au_{99}(SPh)_{42}$. The formula was determined by electrospray ionization and matrix-assisted laser desorption ionization mass spectrometry in conjunction with thermogravimetric analysis. The optical spectrum of $Au_{99}(SPh)_{42}$ nanoclusters shows absorption peaks at ~920 nm (1.35 eV), 730 nm (1.70 eV), 600 nm (2.07 eV), 490 nm (2.53 eV), and 400 nm (3.1 eV) in contrast to conventional gold nanoparticles, which exhibit a plasmon resonance band at 520 nm (for spherical particles). The ceria-supported $Au_{99}(SPh)_{42}$ nanoclusters were utilized as a catalyst for chemoselective hydrogenation of nitrobenzaldehyde to nitrobenzyl alcohol in water using H_2 gas as the hydrogen source. The selective hydrogenation of the aldehyde group catalyzed by nanoclusters is a surprise because conventional nanogold catalysts instead give rise to the product resulting from reduction of the nitro group. The $Au_{99}(SPh)_{42}/CeO_2$ catalyst gives high catalytic activity for a range of nitrobenzaldehyde derivatives and also shows excellent recyclability due to its thermal robustness. We further tested the size-dependent catalytic performance of $Au_{25}(SPh)_{18}$ and $Au_{36}(SPh)_{24}$ nanoclusters, and on the basis of their crystal structures we propose a molecular adsorption site for nitrobenzaldehyde. The nanocluster material is expected to find wide application in catalytic reactions.

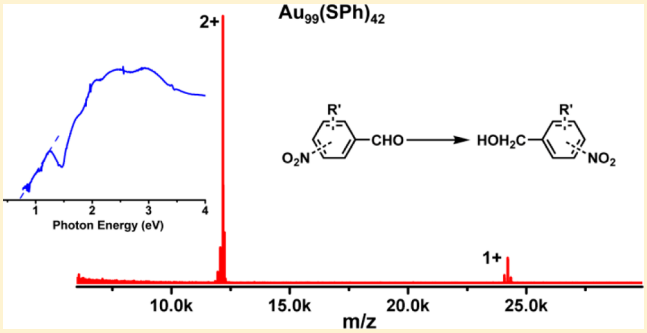

INTRODUCTION

Gold nanoclusters protected by thiolate ligands have emerged as a new class of nanomaterials in recent years.[1−7] Such nanoclusters have attracted wide research interest because of their promising applications, such as catalysis, sensing, and photovoltaics.[8−14] A number of size-discrete, atomically precise gold nanoclusters have been reported,[15−23] such as $Au_{25}(SR)_{18}$, $Au_{36}(SR)_{24}$, $Au_{38}(SR)_{24}$, $Au_{102}(SR)_{44}$, $Au_{144}(SR)_{60}$, etc. With respect to catalysis by nanoclusters, a major goal is to achieve a fundamental understanding of the size dependence and correlation between the catalytic properties and the nanocluster structure. The $Au_n(SR)_m$ nanoclusters (where n and m represent the numbers of gold atoms and thiolate ligands, respectively) exhibit high stability, and some of them have been crystallographically characterized.[2,16,17,24−26]

In recent research, gold has been reported to exhibit good catalytic performance in reactions such as selective oxidation, hydrogenation, and C−C coupling reactions.[9,27−33] In the hydrogenation reactions, Zhu et al.[31] found that free or oxide-supported $Au_{25}(SR)_{18}$ nanoclusters can be applied in the chemoselective hydrogenation of α,β-unsaturated aldehydes to the corresponding α,β-unsaturated alcohols using H_2 gas as the reducing agent in toluene as the solvent. Scott and co-workers reported stable and recyclable $Au_{25}(SR)_{18}$ nanoclusters for the reduction of 4-nitrophenol to 4-aminophenol using $NaBH_4$ as the hydrogen source and tetrahydrofuran (THF) as the solvent.[33] On the other hand, conventional gold nanoparticles have also been utilized in catalytic hydrogenation reactions, and there have been a few reports of the use of supported gold nanoparticle catalysts for reducing aldehydes to alcohols as well as reducing nitro groups to amine groups.[34−40] In principle, nitrobenzaldehyde could be reduced to three major products: aminobenzaldehyde, nitrobenzyl alcohol, and aminobenzyl alcohol (Scheme 1). For example, Corma and Serna reported the chemoselective hydrogenation of *p*-nitrobenzaldehyde to *p*-aminobenzaldehyde with 97% selectivity using oxide-supported gold nanoparticles (e.g., Au/TiO_2 and Au/Fe_2O_3) as catalysts and H_2 (10−25 bar) as the reducing agent under thermal conditions (T > 100 °C).[35] Compared with the conventional Au/oxide catalysts, ultrasmall (<2 nm) and nonmetallic $Au_n(SR)_m$ nanoclusters may exhibit different catalytic properties in the selective hydrogenation of nitrobenzaldehyde and its derivatives.[9]

Scheme 1. General Pathways for Reduction of Nitrobenzaldehyde Catalyzed by Gold Nanocatalysts

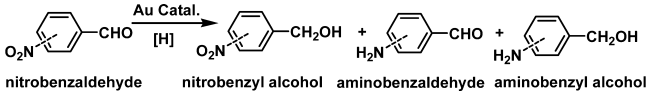

Received: January 6, 2014
Published: February 25, 2014

   dx.doi.org/10.1021/ja500121v | *J. Am. Chem. Soc.* 2014, 136, 3673−3679

Here we report the synthesis of thermally robust, atomically precise gold nanoclusters formulated as $Au_{99}(SPh)_{42}$ and their catalytic application in the chemoselective hydrogenation of nitrobenzaldehyde to nitrobenzyl alcohol in water under mild conditions (80 °C) using H_2 (20 bar) as the hydrogen source. High chemoselectivity (~100%) for the nitrobenzyl alcohol product has been attained, in contrast to the reduction of the nitro group reported previously.[35] The use of water as the solvent is advantageous compared with the previously reported catalytic hydrogenation process. To the best of our knowledge, this is the first report of the synthesis of the $Au_{99}(SR)_{42}$ nanoclusters and their application in chemoselective hydrogenation.

RESULTS AND DISCUSSION

Synthesis and Characterization of the $Au_{99}(SPh)_{42}$ Nanoclusters. The nanoclusters were synthesized via two primary steps. In the first step, polydispersed Au nanoclusters protected by phenylthiolate ligands (−SPh) were prepared at a thiol/Au ratio of 2.0 in dichloromethane. These polydispersed nanoclusters were then used as the precursor for the second step. Briefly, the polydispersed Au nanoclusters were dissolved in 1 mL of toluene and then etched with 1 mL of neat thiophenol (HSPh) at 80 °C overnight. A size-focusing process[41] occurred during the reaction. Matrix-assisted laser desorption ionization mass spectrometry (MALDI-MS) analysis of the product showed a single species with mass at ~24 kDa (vide infra). The final $Au_n(SPh)_m$ product was obtained after removal of excess thiol and Au(I)−SR byproduct (poorly soluble in most solvents); details are provided in the Experimental Section. To facilitate determination of the formula of the $Au_n(SPh)_m$ product, we also used $HSPhCH_3$ (which differs from HSPh merely by a $-CH_3$ group) to prepare $Au_n(SPhCH_3)_m$ nanoclusters.

Transmission electron microscopy (TEM) imaging of the $Au_n(SPh)_m$ nanoclusters showed the cluster size to be ~1.5 nm (Figure 1). The UV−vis spectrum of the $Au_n(SPh)_m$ nanoclusters shows absorption bands at 730, 600, 490, and 400 nm (Figure 2A), and the $Au_n(SPhCH_3)_m$ nanoclusters show similar peaks (Figure S1 in the Supporting Information). The multiband spectra of the $Au_n(SPh)_m$ and $Au_n(SPhCH_3)_m$ nanoclusters are in contrast with that of conventional gold nanoparticles, which exhibit a plasmon band at 520 nm (for spherical particles). Thus, these nanoclusters are nonmetallic. By extrapolation of the optical absorbance to zero (i.e., to the photon energy scale), the band gap of $Au_{99}(SR)_{42}$ (R = Ph, $PhCH_3$) was determined to be ~0.7 eV (Figure 2A inset), which is smaller than the band gap of 1.3 eV for $Au_{25}(SR)_{18}$ nanoclusters.[24]

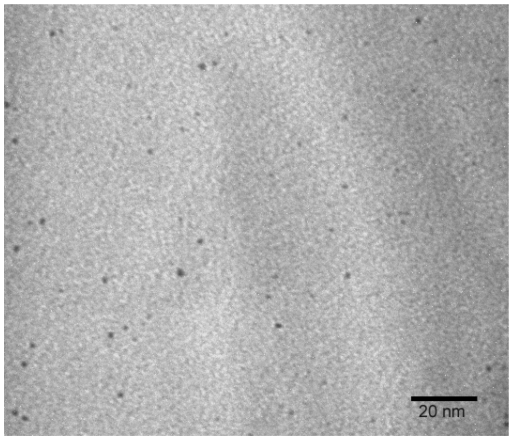

Figure 1. TEM image of $Au_n(SPh)_m$ nanoclusters (diameter ≈ 1.5 nm). The white speckles (pixels) are caused by the high gain setting of the CCD camera in TEM imaging. Scale bar = 20 nm.

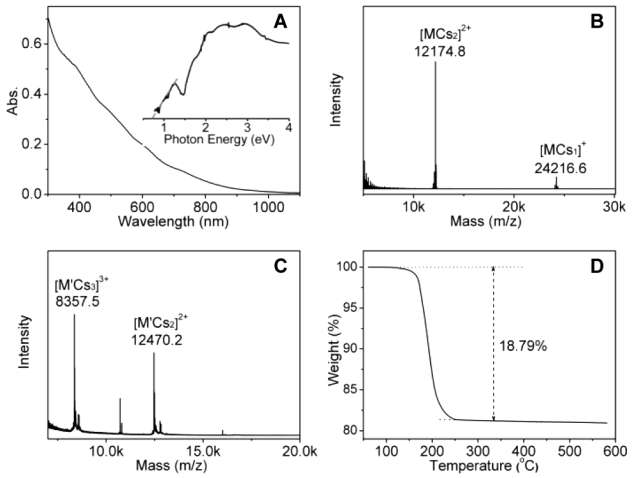

Figure 2. (A) Optical spectrum of $Au_n(SPh)_m$ nanoclusters dissolved in dichloromethane. The inset shows the photon energy plot. (B) ESI mass spectrum of the $Au_n(SPh)_m$ product (denoted as M). (C) ESI mass spectrum of the $Au_n(SPhCH_3)_m$ product (denoted as M′). (D) TGA curve of the $Au_n(SPh)_m$ nanoclusters (under a N_2 atmosphere). In (B) and (C), k = 1000.

To determine the exact molecular mass and formula of the $Au_n(SPh)_m$ nanoclusters, we performed electrospray ionization mass spectrometry (ESI-MS) analysis. ESI is a much softer ionization method than MALDI.[19,42] To impart charges to the nanocluster, cesium acetate (CsOAc) was added to the cluster solution. During the ESI process, Cs^+ ions were attached to the cluster, forming positively charged $[\text{cluster} + Cs_x]^{x+}$ adducts. In the ESI-MS analysis of $Au_n(SPh)_m$ (hereafter denoted as M), peaks centered at m/z 24216.6 and 12174.8 were observed (Figure 2B). The ratio of the first peak to the second is close to 2 (24216.6/12174.8 = 1.99), implying that the first peak is a 1+ charged $[MCs_1]^+$ adduct and the second peak is a 2+ charged $[MCs_2]^{2+}$ adduct.

ESI-MS analysis of the $-SPhCH_3$-protected nanocluster (denoted as M′) was also done. Two main peaks centered at m/z 8357.5 and 12470.2 were observed (Figure 2C), and their ratio is close to 1.5 (i.e., 12470.2/8357.5 = 1.49), which implies 3+ charged $[M'Cs_3]^{3+}$ and 2+ charged $[M'Cs_2]^{2+}$ adducts, respectively. The peak at m/z ~10.7k is an impurity in the $Au_n(SPhCH_3)_m$ sample (this sample was only used for cross-determination of the cluster formula, not for the catalytic experiment). The UV−vis spectrum of $Au_n(SPhCH_3)_m$ is identical to that of $Au_n(SPh)_m$, which indicates that the two nanoclusters are the same size (i.e., have the same values of n and m).

Herein we chose the doubly charged $[MCs_2]^{2+}$ and $[M'Cs_2]^{2+}$ nanoclusters for cross-determination of their formula.[6,20] The two ligands differ merely by a mass difference of 14.02 Da. The ESI peak value for doubly charged $[Au_n(SPhCH_3)_mCs_2]^{2+}$ minus that for $[Au_n(SPh)_mCs_2]^{2+}$ is Δ_{peak} = 12470.2 − 12174.8 = 295.4, and thus, the precise number of ligands is $m = \Delta_{peak} \times (\text{ion charge})/(\text{mass difference}) = 295.4 \times 2/14.02 = 42.14$; accordingly, the

dx.doi.org/10.1021/ja500121v | J. Am. Chem. Soc. 2014, 136, 3673−3679

number of gold atoms n is determined to be 99.07. Therefore, the molecular formula of the $Au_n(SR)_m$ nanoclusters is $Au_{99}(SR)_{42}$. The two ESI peaks in Figure 2B are assigned to $[Au_{99}(SPh)_{42}Cs]^+$ (theoretical m/z 24217.7; deviation 1.1) and $[Au_{99}(SPh)_{42}Cs_2]^{2+}$ (theoretical m/z 12175.2; deviation −0.6). Similarly, the two ESI peaks in Figure 2C are $[Au_{99}(SPhCH_3)_{42}Cs_2]^{2+}$ (theoretical m/z 12469.9; deviation 0.3) and $[Au_{99}(SPhCH_3)_{42}Cs_3]^{3+}$ (theoretical m/z 8357.6; deviation −0.1). With the molecular masses of $Au_{99}(SPh)_{42}$ and $Au_{99}(SPhCH_3)_{42}$ precisely matching with the ESI-MS results, the formula of the new nanoclusters was unequivocally determined to be $Au_{99}(SR)_{42}$. Thermogravimetric analysis (TGA) was also performed (Figure 2D) and showed a weight loss of 18.79 wt % (corresponding to thiolate ligands) at ∼200 °C, consistent with the value expected according to the formula $Au_{99}(SPh)_{42}$ (19.0 wt %). The pure $Au_{99}(SPh)_{42}$ nanoclusters were further utilized in catalytic hydrogenation.

Catalytic Performance of the $Au_{99}(SPh)_{42}$ Nanoclusters. The catalytic hydrogenation reaction was carried out under mild conditions (80 °C for 4 h), and the reaction product was analyzed by NMR spectroscopy. Using free (i.e., unsupported) $Au_{99}(SPh)_{42}$ nanoclusters as the catalyst, we obtained 8.7% conversion of 4-nitrobenzaldehyde with ∼100% selectivity for 4-nitrobenzyl alcohol (Table 1, entry 1). The selective hydrogenation of the aldehyde group (rather than the nitro group as reported by Corma and Serna[35]) is remarkable and implies new catalytic properties of the $Au_n(SR)_m$ nanoclusters compared with conventional gold nanocatalysts. It is worth noting that the UV−vis spectrum of the $Au_{99}(SPh)_{42}$ nanocluster catalyst after the hydrogenation reaction was the same as that of the starting $Au_{99}(SPh)_{42}$ nanocluster (Figure 3A), indicating that the nanoclusters were robust and intact

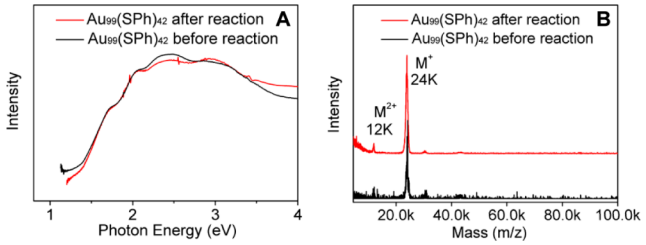

Figure 3. (A) Optical spectra and (B) MALDI-MS spectra of $Au_{99}(SPh)_{42}$ nanoclusters before and after the catalytic hydrogenation reaction.

after the catalytic reaction; this was further confirmed by MALDI-MS analysis of the $Au_{99}(SPh)_{42}$ nanocluster catalyst before and after the reaction, which showed the same sharp peak centered at ∼24 kDa (Figure 3B). In addition, TEM imaging of the nanoclusters after the catalytic reaction also confirmed that there was no change in size (Figure S3 in the Supporting Information).

Support Effects. Loading of nanogold catalysts on oxide supports can often provide large enhancements in the catalytic activity (e.g., conversion and/or selectivity).[43−45] In this work, we chose three different oxides (i.e., SiO_2, TiO_2, and CeO_2) as supports for the $Au_{99}(SPh)_{42}$ nanoclusters to improve the catalytic activity. The loading of $Au_{99}(SPh)_{42}$ on the oxide-supported catalysts was ∼1 wt %. The supported catalysts were prepared by impregnation of oxide powders in a dichloromethane solution of $Au_{99}(SPh)_{42}$ followed by centrifugation, drying under vacuum, and annealing for 1 h at 150 °C (below the ligand desorption temperature of 200 °C; see Figure 2D). To confirm that the nanoclusters did not decompose at 150 °C, we performed an isothermal analysis of unsupported $Au_{99}(SPh)_{42}$ nanoclusters at 150 °C for 1 h in an atmosphere of air (Figure S2A in the Supporting Information). No weight loss was observed, indicating that the phenylthiolate ligands still remained on the cluster surface during the annealing process at 150 °C. The UV−vis spectrum of $Au_{99}(SPh)_{42}$ also showed no changes after the 150 °C thermal treatment (Figure S2B in the Supporting Information).

The supported $Au_{99}(SPh)_{42}$ nanocluster catalysts were then used in catalytic chemoselective hydrogenation reactions under reaction conditions identical to those in the above case of the unsupported nanocluster catalyst (see notes in Table 1), except

Table 1. Hydrogenation of 4-Nitrobenzaldehyde to 4-Nitrobenzyl Alcohol Using Free and Supported $Au_{99}(SPh)_{42}$ Nanoclusters as Catalysts[a]

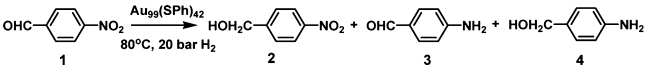

			selectivity (%)[b]		
entry	support	conv. (%)[b]	2	3	4
1[c]	none	8.7	100	n.d.	n.d.
2	SiO_2	27.9	100	n.d.	n.d.
3	TiO_2	69.8	100	n.d.	n.d.
4	CeO_2	93.1	100	n.d.	n.d.
5[d]	CeO_2	92.9	100	n.d.	n.d.
6[e]	CeO_2	93.4	100	n.d.	n.d.

[a]Reaction conditions: $Au_{99}(SPh)_{42}$/oxide (100 mg, 1 wt % loading) catalyst in 1 mL of H_2O, 0.05 mmol of 4-nitrobenzaldehyde, 0.1 mmol of pyridine, 20 bar H_2, 80 °C, 12 h. [b]The conversion (conv.) of 4-nitrobenzaldehyde and selectivity for 4-nitrobenzyl alcohol were determined by NMR analysis. The conversion and selectivity values are averages over three measurements (error bar: ∼0.5%). n.d. = not detected. [c]Reaction conditions: 1 mg of free $Au_{99}(SPh)_{42}$ nanoclusters in 1 mL of toluene, 0.1 mL of H_2O, 0.05 mmol of 4-nitrobenzaldehyde, 0.1 mmol of pyridine, 20 bar H_2, 80 °C, 4 h. [d]Second reuse. [e]Third reuse.

that H_2O was used as the solvent and the reaction time was prolonged to 12 h. It was found that the conversion increased to 27.9% using $Au_{99}(SPh)_{42}/SiO_2$ as the catalyst (Table 1, entry 2), 69.8% using $Au_{99}(SPh)_{42}/TiO_2$ (entry 3), and 93.1% using $Au_{99}(SPh)_{42}/CeO_2$ (entry 4), while the chemoselectivity for the 4-nitrobenzyl alcohol product was maintained at ∼100% in all the three cases. These results suggest that the cluster catalysts are influenced by the acid/base properties of the oxide supports. Among the supports, SiO_2 is acidic while TiO_2 is amphoteric and CeO_2 is basic.

We also investigated the recyclability of the $Au_{99}(SPh)_{42}/CeO_2$ catalyst. In this test, the $Au_{99}(SPh)_{42}/CeO_2$ catalyst was recovered after the reaction by centrifugation (1000 rpm for 5 min), washed with water and ethyl acetate, and dried in vacuum. A fresh reaction was run with reactants in fresh solvent under identical conditions using the recycled catalyst. Indeed, the recycled catalyst showed the same activity and selectivity as the fresh catalyst (Table 1, entries 5 and 6). No appreciable loss of catalytic activity and selectivity was observed after three cycles (more cycles were not tested). Thus, the $Au_{99}(SPh)_{42}/CeO_2$ catalyst is practically useful in the chemoselective hydrogenation process.

dx.doi.org/10.1021/ja500121v | J. Am. Chem. Soc. 2014, 136, 3673−3679

Scope of the Catalytic Reaction: Nitrobenzaldehyde Derivatives. Furthermore, we investigated the catalytic activity of $Au_{99}(SPh)_{42}/CeO_2$ for a range of substrates with aldehyde and nitro groups (Table 2). First, we examined the effect of

Table 2. Chemoselective Hydrogenation of a Range of Substrates with Nitro and Aldehyde Groups Using $Au_{99}(SPh)_{42}/CeO_2$ as the Catalyst[a]

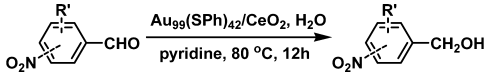

Entry	Substrate	Product	Conv. (%)	Select. (%)
1	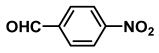	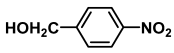	93.1	100
2	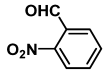	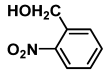	73.2	100
3	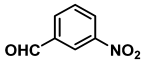	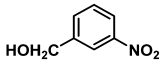	98.5	100
4	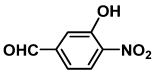	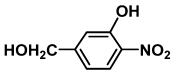	84.1	100
5	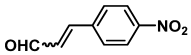	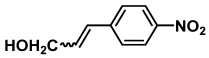	90.0	100
6	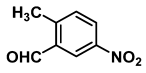	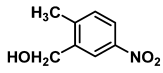	98.9	100
7	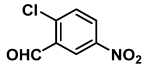	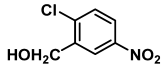	99.5	100

[a]The reaction conditions were the same as in Table 1.

placing the nitro group at the ortho, meta, or para position, and it was clearly shown that *m*-nitrobenzaldehyde gave the best results among the three nitrobenzaldehyde reactants (entries 1−3). We also tested the effect of electronic factors of the substrates (including methyl, hydroxyl, and chloro groups) on the reactant conversion and the selectivity for alcohol products. The inclusion of methyl and chloro groups had no effect on the hydrogenation reaction within the experimental error of ∼0.5% (entries 6 and 7), while the conversion was strongly affected by the presence of the hydroxyl group (entry 4). We also expanded the substrate to 3-(4-nitrophenyl)-2-propenal (which has an extended π system), and indeed, 90.0% conversion was obtained (entry 5) and the C=C bond was not reduced under our conditions. It is interesting that the selectivity for the nitrobenzyl alcohol was ∼100% in all of the above hydrogenation reactions. Overall, the catalytic activity of the $Au_{99}(SPh)_{42}/CeO_2$ catalyst was considerably influenced by electrophilic aromatic substitution but not by electron-rich or -deficient side groups.

Size Dependence. To investigate the potential size dependence, we prepared two smaller gold nanoclusters, $Au_{25}(SPh)_{18}$ and $Au_{36}(SPh)_{24}$, protected by the same phenylthiolate ligand as in $Au_{99}(SPh)_{42}$. The two gold nanoclusters were characterized by UV−vis and MALDI-MS or ESI-MS. In the case of $Au_{25}(SPh)_{18}$ nanoclusters, optical absorption peaks characteristic of $Au_{25}(SR)_{18}$ nanoclusters[24,25] were observed at 650, 450, and 400 nm (Figure 4A), and MALDI-MS analysis (Figure 4B) showed a clean signal at *m*/*z* 6889.4 [theoretical value for $Au_{25}(SPh)_{18}$: 6889.1]. Of note, a fragment of

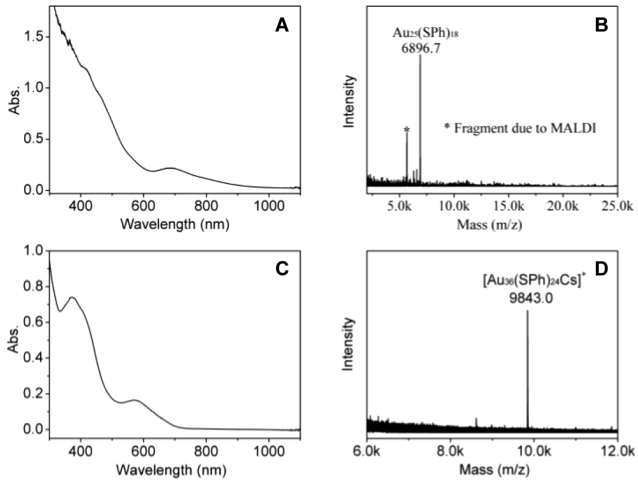

Figure 4. (A, C) Optical spectra of (A) $Au_{25}(SPh)_{18}$ and (C) $Au_{36}(SPh)_{24}$ nanoclusters (both in dichloromethane). (B) MALDI-MS spectrum of $Au_{25}(SPh)_{18}$ nanoclusters (positive mode). (D) ESI-MS spectrum of the $Au_{36}(SPh)_{24}$ nanoclusters. The peak marked with an asterisk (*) in (B) is a fragment caused by MALDI.

$Au_{25}(SPh)_{18}$ caused by MALDI was observed at 5664.9 and was assigned to $Au_{21}(SPh)_{14}$, obtained by loss of a $Au_4(SPh)_4$ unit from $Au_{25}(SPh)_{18}$. For the $Au_{36}(SPh)_{24}$ nanocluster, two optical absorption peaks were observed at 370 and 580 nm (Figure 4C), which are consistent with the reported spectrum of pure $Au_{36}(SR)_{24}$.[16] ESI-MS analysis of the clusters showed a single signal at *m*/*z* 9843.0 (Figure 4D), which is assigned to the adduct peak of $[Au_{36}(SPh)_{24}Cs]^+$ (theoretical *m*/*z*: 9843.4).

The catalytic performance of $Au_{25}(SPh)_{18}$ and $Au_{36}(SPh)_{24}$ nanoclusters was tested under the same reaction conditions as noted in Table 1 for the $Au_{99}(SPh)_{42}$ nanoclusters. Their catalytic performance was compared on the basis of equal amounts of nanoclusters [0.04 μmol of $Au_n(SPh)_m$ nanoclusters in all reactions]. We obtained conversions of 13.5% and 13.0% of 4-nitrobenzaldehyde with free $Au_{25}(SPh)_{18}$ and $Au_{36}(SPh)_{24}$ nanoclusters, respectively (Table 3, entries 1 and 2); in both cases, the selectivity for the product was ∼100%. Similar to the $Au_{99}(SPh)_{42}$ nanocluster catalyst, $Au_{25}(SPh)_{18}$ and $Au_{36}(SPh)_{24}$ catalysts were sufficiently robust and remained intact after the

Table 3. Effect of the Size of the Unsupported and Ceria-Supported $Au_n(SPh)_m$ Nanoclusters on the Hydrogenation of 4-Nitrobenzaldehyde; The Catalytic Performance Is Compared on an Equal Cluster Molar Basis

entry	catalyst	conv. (%)[a]
1[b]	$Au_{25}(SPh)_{18}$	13.5
2[b]	$Au_{36}(SPh)_{24}$	13.0
3[b]	$Au_{99}(SPh)_{42}$	8.9
4[c]	$Au_{25}(SPh)_{18}/CeO_2$	98.5
5[c]	$Au_{36}(SPh)_{24}/CeO_2$	97.6
6[c]	$Au_{99}(SPh)_{42}/CeO_2$	93.1

[a]The conversion of 4-nitrobenzaldehyde was determined by NMR analysis. [b]Reaction conditions: 0.04 μmol of free $Au_n(SPh)_m$ nanoclusters in 1 mL of toluene, 0.1 mL of H_2O, 0.05 mmol of 4-nitrobenzaldehyde, 0.1 mmol of pyridine, 20 bar H_2, 80 °C, 4 h. [c]Reaction conditions: $Au_n(SPh)_m$/oxide catalysts (1 wt % loading, 0.04 μmol of $Au_n(SPh)_m$ nanoclusters in all cases) in 1 mL of H_2O, 0.05 of mmol 4-nitrobenzaldehyde, 0.1 mmol of pyridine, 20 bar H_2, 80 °C, 12 h.

dx.doi.org/10.1021/ja500121v | J. Am. Chem. Soc. 2014, 136, 3673−3679

hydrogenation reaction, as evidenced by the UV−vis spectra and MALDI-MS analyses (Figures S4 and S5 in the Supporting Information). With CeO_2-supported $Au_{25}(SPh)_{18}$ and $Au_{36}(SPh)_{24}$ nanocluster catalysts, the catalytic performance was significantly improved (e.g., conversion >97%; entries 4 and 5), similar to the case of $Au_{99}(SPh)_{42}/CeO_2$. The catalytic performance of these three sizes of $Au_n(SPh)_m$ nanoclusters is comparable on the cluster molar basis, and the turnover frequency (TOF) can reach up to 97−100 h^{-1} (i.e., moles of product per hour per mole of clusters) on the supported $Au_n(SPh)_m/CeO_2$ catalysts versus 28−42 h^{-1} over the unsupported $Au_n(SPh)_m$ nanoclusters.

Mechanistic Insights. The $Au_{36}(SR)_{24}$ and $Au_{25}(SR)_{18}$ nanoclusters have been crystallographically characterized in previous reports.[16,24,25] Each $Au_{25}(SR)_{18}$ nanocluster consists of an icosahedral Au_{13} kernel protected by six −S(R)−Au−S(R)−Au−S(R)− staplelike motifs (Scheme 2A), and the $Au_{36}(SR)_{24}$ structure comprises a truncated tetrahedral Au_{28} kernel protected by four −S(R)−Au−S(R)−Au−S(R)− staples and 12 simple bridging thiolates (Scheme 2B). In previous work on $Au_{25}(SR)_{18}$-catalyzed reduction of CO_2, density functional theory (DFT) simulations of the CO_2 adsorption identified that one carbonyl group of O═C═O adsorbs to the surface gold atoms in the −S(R)−Au−S(R)−Au−S(R)− staples.[10] Following this model, herein we propose that the O═C(H)− group of nitrobenzaldehyde adsorbs onto the exposed gold sites in the staple motifs of $Au_{25}(SR)_{18}$ (Scheme 2C) and similarly in the case of $Au_{36}(SR)_{24}$ (Scheme 2D). While the crystal structure of $Au_{99}(SR)_{42}$ has not been attained, staplelike surface motifs are expected to be present in $Au_{99}(SR)_{42}$, and the O═C(H)− adsorption mode should be similar. Future work will provide further insight into the molecular activation pathways in the chemoselective hydrogenation reaction.

Scheme 2. (A, B) Crystal Structures[16,24,25] of (A) $Au_{25}(SCH_2CH_2Ph)_{18}$ and (B) $Au_{36}(SPh^tBu)_{24}$; (C, D) Corresponding Proposed Nitrobenzaldehyde Adsorption Modes

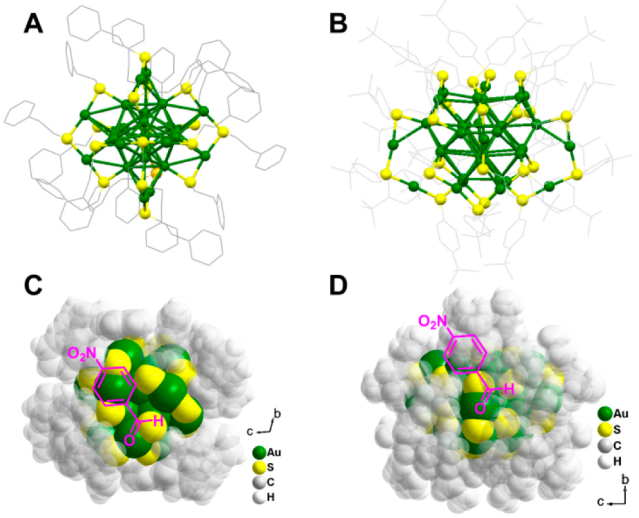

CONCLUSION

We have successfully synthesized thermally robust $Au_{99}(SPh)_{42}$ nanoclusters for catalytic application in the chemoselective hydrogenation of nitrobenzaldehyde and its derivatives. ESI-MS in conjunction with other analyses has unequivocally determined the formula of the nanocluster. The free and oxide-supported $Au_{99}(SPh)_{42}$ nanoclusters catalyze the hydrogenation of nitrobenzaldehyde to nitrobenzyl alcohol with ∼100% chemoselectivity using H_2 gas as the hydrogen source and water as the solvent. The selective hydrogenation of the aldehyde group (as opposed to the nitro group) is attributed to the new catalytic properties of $Au_n(SR)_m$ nanoclusters compared to conventional gold nanocatalysts. The $Au_{99}(SPh)_{42}$ nanocluster catalysts remain intact after the chemoselective hydrogenation process at 80 °C. A large promotional effect of oxide supports was observed in the hydrogenation reaction, and CeO_2 was found to be the best owing to its basic nature among the three investigated oxide supports (i.e., SiO_2, TiO_2, and CeO_2). Moreover, the catalyst showed excellent durability. In terms of the cluster size effect, the catalytic performances of CeO_2-supported nanoclusters of different sizes (including $Au_{25}(SPh)_{18}$, $Au_{36}(SPh)_{24}$, and $Au_{99}(SPh)_{42}$) are comparable on a cluster molar basis and the TOF reaches ∼100 h^{-1} (i.e., moles of product per hour per mole of clusters). Future atomic-level understanding of the bonding effect of surface atoms, the electronic properties, and the support effect on the catalytic properties of gold nanoclusters will eventually contribute to the design of highly selective nanocatalysts for specific reactions.

EXPERIMENTAL SECTION

Chemicals. Tetrachloroauric(III) acid ($HAuCl_4·3H_2O$) (99.99% metal basis, Aldrich), tetraoctylammonium bromide (TOAB) (98%, Fluka), sodium borohydride (99.99% metals basis, Aldrich), thiophenol (99%, Sigma-Aldrich), toluene (HPLC grade, 99.9%, Aldrich), methanol (absolute, 200 proof, Pharmco), methylene chloride (HPLC grade, 99.9%, Sigma-Aldrich), and acetone (HPLC grade, 99.9%, Sigma-Aldrich) were obtained from the indicated suppliers. All chemicals were used as received. Nanopure water (resistivity 18.2 MΩ cm) was purified with a Barnstead NANOpure deionized water system. All glassware was thoroughly cleaned with aqua regia (3:1 v/v HCl/HNO_3), rinsed with copious Nanopure water, and then dried in an oven prior to use.

Synthesis and Characterization of $Au_{99}(SR)_{42}$ (R = SPh, $SPhCH_3$) Nanoclusters. $HAuCl_4·3H_2O$ (0.21 mmol, dissolved in 10 mL of water) and TOAB (0.24 mmol, dissolved in 15 mL of dichloromethane) were combined in a three-neck round-bottom flask. The solution was vigorously stirred (∼600 rpm) to facilitate phase transfer of the Au(III) salt into the organic phase. After 15 min, phase transfer was completed; the aqueous layer was removed, and the organic layer was washed with water (2 × 10 mL). Thiol (2.0 equiv relative to gold) was added. The solution color slowly changed from deep red to light yellow. After 1 h, 5 mL of an aqueous solution of $NaBH_4$ (10 equiv relative to gold) was rapidly added to the solution. After $NaBH_4$ addition, the reaction was allowed to proceed overnight. The organic phase was then removed and washed with methanol. The black solid was extracted with 1 mL of toluene and transferred to a flask. Thiol (1 mL) was added, and the solution was heated to 80 °C and maintained at this temperature overnight. During the long-time etching process, the initial polydisperse $Au_n(SR)_m$ nanoclusters were finally converted to monodisperse $Au_{99}(SR)_{42}$ clusters. The organic phase was thoroughly washed with methanol to remove excess thiol, after which the pure $Au_{99}(SR)_{42}$ nanoclusters were simply extracted with dichloromethane.

Characterization of Gold Nanoclusters. TEM images of the nanoclusters were obtained on a Hitachi 7000 transmission electron microscope operated at 75 kV. The specimen was made by placing one drop of a CH_2Cl_2 solution of nanoclusters onto a carbon thin-film-coated TEM grid. The optical spectra of the clusters (dissolved in CH_2Cl_2) were acquired on a Hewlett-Packard Agilent 8453 diode array spectrophotometer (190−1100 nm) and a Varian Cary 5000

dx.doi.org/10.1021/ja500121v | J. Am. Chem. Soc. 2014, 136, 3673−3679

UV−vis−NIR spectrophotometer (190−1600 nm) at room temperature. MALDI-MS was performed with a PerSeptive Biosystems Voyager DE super-STR time-of-flight (TOF) mass spectrometer. *trans*-2-[3-(4-*tert*-Butylphenyl)-2-methyl-2-propenylidene]-malononitrile (DCTB) was used as the matrix in MALDI analysis.[23] Typically, 1 mg of matrix and 0.1 mL of analyte stock solution were mixed in 100 μL of CH_2Cl_2, and 10 μL of this solution was applied to the steel plate and then air-dried prior to MALDI analysis. ESI-MS was performed using a Waters Q-TOF mass spectrometer equipped with a Z-spray source. The sample was dissolved in toluene (1 mg/mL) and then mixed 1:1 (v/v) with a dry methanol solution of CsOAc (50 mM). TGA was conducted on ∼2 mg samples under a N_2 atmosphere (flow rate ∼50 mL/min) on a TG/DAT 6300 analyzer (Seiko Instruments, Inc.) at a heating rate of 10 °C/min.

Typical Procedure for Chemselective Hydrogenation of Nitrobenzaldehyde. In a typical selective hydrogenation reaction, 4-nitrobenzaldehyde (0.05 mmol), pyridine (0.1 mmol), and $Au_{99}(SPh)_{42}$ nanoclusters (∼1 mg) or $Au_{99}(SPh)_{42}$/oxide (100 mg, 1 wt % loading) were added to a reactor (Parr Instrument Company, series 4700, 22 mL capacity) under 20 bar H_2. The reaction mixture was kept at 80 °C as indicated in Table 1. After the reaction, the mixture was extracted with ethyl acetate. The crude product was obtained after removal of the solvent. The conversion of 4-nitrobenzaldehyde and the selectivity for the 4-nitrobenzyl alcohol product were determined by ^{1}H NMR (300 MHz) spectroscopic analysis (Figure S6 in the Supporting Information). In the recycling tests, the $Au_{99}(SPh)_{42}/CeO_2$ catalyst was collected after the reaction by centrifugation at 1000 rpm for 5 min and then reused in a fresh reaction. The reported conversion and selectivity values were averaged over three measurements, and the error is ∼0.5%.

■ ASSOCIATED CONTENT

Supporting Information

UV−vis spectrum of the $Au_n(SPhCH_3)_m$ nanoclusters, isothermal stability analysis at 150 °C and UV−vis spectra of the nanoclusters before/after 150 °C thermal treatment, TEM image of $Au_{99}(SPh)_{42}$ nanoclusters after the catalytic reaction, UV−vis and MALDI-MS spectra of $Au_{25}(SPh)_{18}$ and $Au_{36}(SPh)_{24}$ nanoclusters before and after hydrogenation reaction, and ^{1}H NMR data. This material is available free of charge via the Internet at http://pubs.acs.org.

■ AUTHOR INFORMATION

Corresponding Author

rongchao@andrew.cmu.edu

Notes

The authors declare no competing financial interest.

■ ACKNOWLEDGMENTS

This work was financially supported by the U.S. Department of Energy, Office of Basic Energy Sciences (Grant DE-FG02-12ER16354). We thank Joseph Suhan for assistance with TEM imaging of nanoclusters.

■ REFERENCES

(1) Qian, H.; Zhu, M.; Wu, Z.; Jin, R. *Acc. Chem. Res.* **2012**, *45*, 1470−1479.

(2) (a) Das, A.; Li, T.; Nobusada, K.; Zeng, C.; Rosi, N. L.; Jin, R. *J. Am. Chem. Soc.* **2013**, *135*, 18264−18267. (b) Zeng, C.; Li, T.; Das, A.; Rosi, N. L.; Jin, R. *J. Am. Chem. Soc.* **2013**, *135*, 10011−10013.

(3) Templeton, A. C.; Wuelfing, W. P.; Murray, R. W. *Acc. Chem. Res.* **2000**, *33*, 27−36.

(4) Whetten, R. L.; Shafigullin, M. N.; Khoury, J. T.; Schaaff, T. G.; Vezmar, I.; Alvarez, M. M.; Wilkinson, A. *Acc. Chem. Res.* **1999**, *32*, 397−406.

(5) Maity, P.; Xie, S.; Yamauchi, M.; Tsukuda, T. *Nanoscale* **2012**, *4*, 4027−4037.

(6) Zhu, X.; Jin, S.; Wang, S.; Meng, X.; Zhu, C.; Zhu, M.; Jin, R. *Chem.—Asian J.* **2013**, *8*, 2739−2745.

(7) Malola, S.; Lehtovaara, L.; Knoppe, S.; Hu, K.-J.; Palmer, R. E.; Bürgi, T.; Häkkinen, H. *J. Am. Chem. Soc.* **2012**, *134*, 19560−19563.

(8) Tsukuda, T.; Tsunoyama, H.; Sakurai, H. *Chem.—Asian J.* **2011**, *6*, 736−748.

(9) Li, G.; Jin, R. *Acc. Chem. Res.* **2013**, *46*, 1749−1758.

(10) Kauffman, D. R.; Alfonso, D.; Matranga, C.; Qian, H.; Jin, R. *J. Am. Chem. Soc.* **2012**, *34*, 10237−10243.

(11) Kauffman, D. R.; Alfonso, D.; Matranga, C.; Gao, L.; Jin, R. *J. Phys. Chem. Lett.* **2013**, *4*, 195−202.

(12) Kwak, K.; Kumar, S. S.; Lee, D. *Nanoscale* **2012**, *4*, 4240−4246.

(13) Wu, Z.; Wang, M.; Yang, J.; Zheng, X.; Cai, W.; Meng, G.; Qian, H.; Wang, H.; Jin, R. *Small* **2012**, *8*, 2028−2035.

(14) Sakai, N.; Tatsuma, T. *Adv. Mater.* **2010**, *22*, 3185−3188.

(15) Zhu, M.; Lanni, E.; Garg, N.; Bier, M. E.; Jin, R. *J. Am. Chem. Soc.* **2008**, *130*, 1138−1139.

(16) Zeng, C.; Qian, H.; Li, T.; Li, G.; Rosi, N. L.; Yoon, B.; Barnett, R. N.; Whetten, R. L.; Landman, U.; Jin, R. *Angew. Chem., Int. Ed.* **2012**, *51*, 13114−13118.

(17) Qian, H.; Eckenhoff, W. T.; Zhu, Y.; Pintauer, T.; Jin, R. *J. Am. Chem. Soc.* **2010**, *132*, 8280−8281.

(18) Levi-Kalisman, Y.; Jadzinsky, P. D.; Kalisman, N.; Tsunoyama, H.; Tsukuda, T.; Bushnell, D. A.; Kornberg, R. D. *J. Am. Chem. Soc.* **2011**, *133*, 2976−2982.

(19) Qian, H.; Jin, R. *Nano Lett.* **2009**, *9*, 4083−4087.

(20) Nimmala, P. R.; Yoon, B.; Whetten, R. L.; Landman, U.; Dass, A. *J. Phys. Chem. A* **2013**, *117*, 504−517.

(21) Negishi, Y.; Sakamoto, C.; Ohyama, T.; Tsukuda, T. *J. Phys. Chem. Lett.* **2012**, *3*, 1624−1628.

(22) Tang, Z.; Robinson, D. A.; Bokossa, N.; Xu, B.; Wang, S.; Wang, G. *J. Am. Chem. Soc.* **2011**, *133*, 16037−16044.

(23) Nimmala, P. R.; Dass, A. *J. Am. Chem. Soc.* **2011**, *133*, 9175−9177.

(24) Zhu, M.; Aikens, C. M.; Hollander, F. J.; Schatz, G. C.; Jin, R. *J. Am. Chem. Soc.* **2008**, *130*, 5883−5885.

(25) Heaven, M. W.; Dass, A.; White, P. S.; Holt, K. M.; Murray, R. W. *J. Am. Chem. Soc.* **2008**, *130*, 3754−3755.

(26) Jadzinsky, P. D.; Calero, G.; Ackerson, C. J.; Bushnell, D. A.; Kornberg, R. D. *Science* **2007**, *318*, 430−433.

(27) Julius, M.; Roberts, S.; Fletcher, J. C. Q. *Gold Bull.* **2010**, *43*, 298−306.

(28) Li, Z.; Brouwer, C.; He, C. *Chem. Rev.* **2008**, *108*, 3239−3265.

(29) Li, G.; Liu, C.; Lei, Y.; Jin, R. *Chem. Commun.* **2012**, *48*, 12005−12007.

(30) Li, G.; Jiang, D.; Liu, C.; Yu, C.; Jin, R. *J. Catal.* **2013**, *306*, 177−183.

(31) Zhu, Y.; Qian, H.; Drake, B. A.; Jin, R. *Angew. Chem., Int. Ed.* **2010**, *49*, 1295−1298.

(32) Yamamoto, H.; Yano, H.; Kouchi, H.; Obora, Y.; Arakawa, R.; Kawasaki, H. *Nanoscale* **2012**, *4*, 4148−4154.

(33) Shivhare, A.; Ambrose, S. J.; Zhang, H.; Purves, R. W.; Scott, R. W. J. *Chem. Commun.* **2013**, *49*, 276−278.

(34) Claus, P.; Brückner, A.; Mohr, C.; Hofmeister, H. *J. Am. Chem. Soc.* **2000**, *122*, 11430−11439.

(35) Corma, A.; Serna, P. *Science* **2006**, *313*, 332−334.

(36) Corma, A.; Serna, P.; Garcia, H. *J. Am. Chem. Soc.* **2007**, *129*, 6358−6359.

(37) Ren, D.; He, L.; Yu, L.; Ding, R.-S.; Liu, Y.-M.; Cao, Y.; He, H.; Fan, K. *J. Am. Chem. Soc.* **2012**, *134*, 17592−17598.

(38) Yan, M.; Jin, T.; Chen, Q.; Ho, H. E.; Fujita, T.; Chen, L.; Bao, M.; Chen, M.; Asao, N.; Yamamoto, Y. *Org. Lett.* **2013**, *15*, 1484−1487.

(39) Barrio, L.; Liu, P.; Rodriguez, J. A.; Campos-Martin, J. M.; Fierro, J. L. G. *J. Chem. Phys.* **2006**, *125*, No. 164715.

(40) Ide, M. S.; Hao, B.; Neurock, M.; Davis, R. J. *ACS Catal.* **2012**, *2*, 671−683.

(41) Jin, R.; Qian, H.; Wu, Z.; Zhu, Y.; Zhu, M.; Mohanty, A.; Garg, N. *J. Phys. Chem. Lett.* **2010**, *1*, 2903−2910.
(42) Fields-Zinna, C. A.; Sampson, J. S.; Crowe, M. C.; Tracy, J. B.; Parker, J. F.; de Ney, A. M.; Muddiman, D. C.; Murray, R. W. *J. Am. Chem. Soc.* **2009**, *131*, 13844−13851.
(43) Haruta, M.; Tsubota, S.; Kobayashi, T.; Kageyama, H.; Genet, M. J.; Delmon, B. *J. Catal.* **1993**, *144*, 175−192.
(44) Chng, L. L.; Erathodiyil, N.; Ying, J. Y. *Acc. Chem. Res.* **2013**, *46*, 1825−1837.
(45) Stakheev, A. Y.; Kustov, L. M. *Appl. Catal., A* **1999**, *188*, 3−35.